Accelerated colorimetric immunosensing using surface-modified porous monoliths and gold nanoparticles

Shao-Hsuan Chuag, Guan-Hua Chen, Hsin-Hao Chou, Shu-Wei Shen and Chien-Fu Chen

Graduate Institute of Biomedical Engineering, National Chung Hsing University, Taichung 402, Taiwan

E-mail: stevechen@dragon.nchu.edu.tw

Abstract

A rapid and sensitive immunoassay platform integrating polymerized monoliths and gold nanoparticles (AuNPs) has been developed. The porous monoliths are photopolymerized *in situ* within a silica capillary and serve as solid support for high-mass transport and high-density capture antibody immobilization to create a shorter diffusion length for antibody–antigen interactions, resulting in a rapid assay and low reagent consumption. AuNPs are modified with detection antibodies and are utilized as signals for colorimetric immunoassays without the need for enzyme, substrate and sophisticated equipment for quantitative measurements. This platform has been verified by performing a human IgG sandwich immunoassay with a detection limit of $0.1 \, \text{ng ml}^{-1}$. In addition, a single assay can be completed in 1 h, which is more efficient than traditional immunoassays that require several hours to complete.

1. Introduction

Immunoassays such as enzyme-linked immunosorbent assay (ELISA) and nucleic acid sequence-based amplification (NASBA) are well-established biomolecular detection techniques that are used in aid of drug discovery and disease diagnostics [1–3]. Highly sensitive and selective results can be obtained from strong noncovalent antibody–antigen interactions, and the detection signal of low abundant analytes can be amplified efficiently through the high-turnover catalysis of the detection substrate by enzymes [4]. However, the multiple incubation, washing and blocking steps that take hours to complete would limit the application of the immunoassays for real-time clinical diagnosis and subsequent treatment. In addition, the analyte and reagent consumption is not only costly, but also presents a challenge for clinical samples that are available in limited quantities.

Conventional assays are typically carried out in surface-coated multi-well plates. Because the antibody–antigen interactions occur in open wells, diffusion limits the extent to which antigens can interact with the antibodies that are immobilized on the side of the wells. To increase the assay efficiency and decrease the analyte and reagent consumption, high surface-to-volume ratio materials, such as magnetic microbeads [5–7], polymer microbeads [8, 9], hydrogels [10, 11] and porous monoliths [12, 13] were adopted to anchor larger amounts of primary antibodies. They provide larger surface areas for binding more antibodies per unit assay volume, and they contribute to a shorter diffusion distance between adjacent antibodies; therefore, the analysis time can be decreased from hours to minutes, and higher detection sensitivity and less reagent consumption can be achieved.

Following their successful synthesis and preparation, nanomaterials such as carbon nanotubes (CNT) [14, 15], graphene [16, 17], nanowires [18, 19] and nanoparticles [20, 21] have been widely adopted for multiplex immuno-assays. Nanomaterials function as higher surface-to-volume ratio carriers, and their specific physical and chemical properties increase the versatility of assay platforms such as field-effect transistors (FETs) for label-free biomolecule sensing and detection [15, 16, 18]. However, sophisticated laboratory infrastructure and well-trained operators are needed for the complicated fabrication processes and acquisition of assay results.

Among the nanoparticles that are used for biosensing, gold nanoparticles (AuNPs) are attractive because of their simple preparation method, high stability, biocompatibility and distinctive optical and versatile chemical properties [22–25]. Based on the surface plasmon resonance (SPR) effect, the color of the 13 nm diameter monodispersed colloid AuNPs is red and the absorbance wavelength is centered at approximately 520 nm [25, 26]. Various colorimetric biosensing mechanisms have been developed utilizing the characteristics of absorbance wavelength change in an electrolyte solution [27] and the stronger molar absorptivities than organic dye [28, 29]. However, most of these assays require ∼1 ml volume for a single assay, and the conjugation of biomolecules to AuNP surfaces takes hours to complete.

In this report, we propose a colorimetric immunoassay platform combining photopolymerized monoliths as a high surface-to-volume ratio solid support for antibody binding and AuNP immunoprobes for colorimetric detection signaling. Monoliths are porous structures containing surface groups that can be easily modified [30], and they have been widely used as stationary phases for biochemical separation and analysis [31, 32]. To increase the number of antigen detection sites, porous monoliths are modified to contain a thiol ligand on their surfaces, and then they are reacted with the cysteine sulfhydryl group of capture anti-human IgG (caHIgG) to form intermolecular disulfide bridges between antibodies and the side groups on the monoliths [33]. AuNP immunoprobes are prepared using secondary aHIgG to electrostatically modify the AuNP surfaces [34]. Different concentrations of analytes, human IgG (HIgG), from 0.1 ng ml^{-1} to 1 mg ml^{-1} in phosphate buffered saline (PBS) buffer, were added to an aHIgG–AuNPs solution to form the HIgG–aHIgG–AuNPs complexes. After injecting the solution of HIgG–aHIgG–AuNP complexes into the silica capillary, the HIgG–aHIgG–AuNPs interacted with and were captured by the caHIgG-monolith surfaces beginning from the head of the monolith, resulting in different lengths of monolith segments that changed color from white to dark red according to the amount of HIgG–aHIgG–AuNPs that was bound to the caHIgG monolith. The colorimetric immunosensing platform permits rapid and low reagent-consuming analysis with the potential for cost-effective and portable point-of-care diagnosis applications.

2. Experimental

2.1. Chemicals and reagents

Methanol, ethanol, acetone, acetonitrile, sodium hydroxide, hydrochloric acid, 3-methacryloyloxypropyl trimethoxy-silane, glycidyl methacrylate (GMA), ethylene dimeth-acrylate (EDMA), 2,2-dimethoxy-2-phenylaceto phenone (DMPA), cysteamine, trisodium citrate, bovine serum albumin (BSA), PBS, tris-borate-EDTA (TBE), sodium chloride, TWEEN 20, HIgG, monoclonal anti-HIgG and anti-HIgG (whole molecule) were purchased from Sigma-Aldrich (St Louis, MO). Hydrogen tetrach-loroaurate(III) trihydrate was obtained from Acros (Geel, Belgium).

2.2. Characterization

The morphology of the monoliths was inspected using a scanning electron microscope (SEM; JSM-6700F, JEOL, Tokyo, Japan). The sizes of the synthesized AuNPs were verified by a transmission electron microscope (TEM; H7100, Hitachi High-Technologies, Tokyo, Japan). The concentration of AuNP colloids and the functionalization of aHIgG–AuNPs were characterized optically by UV–Vis spectroscopy (Cintra 10e, GBC, Victoria, Australia). Immunoassay colorimetric results were recorded using a desktop scanner (V370, Seiko Epson Corp., Nagano, Japan) and image analysis was performed using the free software ImageJ (National Institutes of Health, US).

2.3. AuNPs preparation

AuNPs with an average diameter of 13 nm were prepared by citrate reduction of HAuCl$_4$ [38]. A 1 mM HAuCl$_4$ solution (250 ml) was prepared and stirred while boiling. An amount of 25 ml 38.8 mM trisodium citrate was added and refluxed for an additional 15 min. When the color of the solution changed from yellow to deep red, the solution was cooled to room temperature. The concentration of AuNP colloids used in all tests was determined according to the Beer–Lambert law via absorbance measurement [39].

2.4. Formation of photopolymerized monoliths

First, the fused silica capillary was vinylized for monolith anchoring [40]. A homogenized and deaerated mixture consisting of 24 wt % GMA (functional monomer), 16 wt% EDMA (cross-linker), 30 wt% methanol and 30 wt% ethanol (porogens) and 1 wt% DMPA (photoinitiator, with respect to monomers) was then used to fill the vinylized capillary. After sealing both ends with septa, the silica capillary was exposed to UV irradiation using a xenon arc lamp at a power density of 20.0 mW cm^{-2} for 8 min through a photomask. After the monoliths were formed, the silica capillary was rinsed with acetonitrile and nanopure water.

2.5. Monoliths modified with antibodies

The poly(GMA-co-EDMA) monolith was modified with caHIgG antibodies through surface thiol-functionalization and antibody binding processes. A 2.5 M aqueous cysteamine solution was added to the monoliths with a flow rate of $1\,\mu l\,min^{-1}$ for 1 h at room temperature. The monoliths were then rinsed with nanopure water at a flow rate of $3\,\mu l\,min^{-1}$ until the pH of the eluent was neutral.

A $4\,\mu g\,ml^{-1}$ monoclonal caHIgG antibody solution was passed through the monoliths at $5\,\mu l\,min^{-1}$ for 10 min and incubated at room temperature for 10 min. A $5\,\mu l\,min^{-1}$ wash with PBS buffer for 30 min was conducted to remove unbound antibodies from the monoliths. A blocking buffer containing a PBS buffer with 1% BSA and 0.1% TWEEN 20 was pumped into the silica capillary at $5\,\mu l\,min^{-1}$ for 30 min and then incubated for 10 min to eliminate nonspecific binding to the capillary sidewalls and monolith surfaces. Excess blocking buffer and unbound BSA were removed by rinsing with the PBS buffer at $5\,\mu l\,min^{-1}$ for 30 min.

2.6. Formation of antibody conjugated AuNP probes

A modified method described by Parolo *et al* was used to obtain AuNPs conjugated with aHIgG antibodies [34]. The pH of AuNP colloids (15 nM, 1.5 ml) was adjusted to 7.4 using TBE buffer, followed by the addition of $100\,\mu l$ antibody solution $(2\,\mu g\,ml^{-1})$ and a 20 min incubation step. A $100\,\mu l$ aqueous solution of $1\,mg\,ml^{-1}$ BSA in nanopure water was added and incubated for 20 min. The solution was then centrifuged at 14 000 rpm for 20 min. The supernatant was removed and the AuNP pellets were redispersed twice in $500\,\mu l$ 2 mM TBE buffer with sucrose (10 wt%).

2.7. Colorimetric immunoassay

To evaluate the performance of the colorimetric immunoassay, different concentrations of HIgG from $0.1\,ng\,ml^{-1}$ to $1\,mg\,ml^{-1}$ were prepared in PBS buffer. aHIgG–AuNP $(50\,\mu l)$ was incubated with various concentrations of $50\,\mu l$ HIgG solution in an Eppendorf tube for 30 min and infused into the silica capillary at $5\,\mu l\,min^{-1}$ for 10 min. After a 10 min incubation, the excess or unbound HIgG–aHIgG–AuNPs were removed by rinsing with a PBS wash buffer (0.05% Tween 20 in PBS, pH 7.6) at $10\,\mu l\,min^{-1}$ for 10 min. The control experiment was performed according to the aforementioned procedures using aHIgG–AuNPs without HIgG incubation as the analyte.

3. Results and discussion

The strategy of sandwich immunosensing using porous monoliths and AuNPs probes is illustrated in figure 1. First, photopolymerized porous monoliths are modified with caHIgG through intermolecular disulfide bridges or other thiol linkages. Then, the AuNP immunoprobes are prepared via electrostatic binding of the secondary aHIgG to the AuNP surfaces. Following the mixing of the HIgG

molecules and their conjugation with AuNP immunoprobes, the HIgG–aHIgG–AuNPs mixture is injected into the silica capillary and bound to caHIgG on the monolith surfaces beginning from the head of the monolith, which results in different lengths of the monolith segments that change color from white to dark red based on the color of the AuNP immunoprobes and the amount of HIgG antibodies.

3.1. Formation of photopolymerized monoliths

To avoid extraction processes using centrifugation or magnets for bead-based immunoassays, the porous monolith was used as a solid support within the silica capillary. In this study, the porous monoliths were selected as solid supports based on their ease of preparation, high surface area for denser antibodies to be anchored for sensing, multiplex surface modification to form a variety of functional groups on the monolith surfaces, high mass transport and decreased diffusion length requirement for antibody–antigen interaction to enable rapid assay execution and low reagent consumption. These specific characteristics make monoliths strong candidates for solid supports in immunoassays. The morphology of the macroporous poly(GMA-co-EDMA) monolith was analyzed by SEM (figure 1(a)). The SEM image shows that the monoliths possessed homogeneous morphology and consisted of globule clusters that were formed by fused $\sim 1\,\mu m$ diameter globules.

## 3.2. Monoliths modified with antibodies

The proposed reaction route to modify caHIgG antibodies on the monolith surfaces is described in figure 2. The oxirane moieties of poly(GMA-co-EDMA) monoliths are chemically modified into thiol groups to covalently attach caHIgG on the surface via the formation of disulfide bridges [35]. First, cysteamine is used as the nucleophilic reagent to chemically modify the oxirane ring on the pre-treated monoliths to thiol terminal groups [36]. The caHIgG antibodies are then introduced and the thiol groups on the monolith surface react with the cysteine sulfhydryl groups of HIgG to form the intermolecular disulfide bridges or other thiol linkages between the antibodies and the side groups on the monoliths [33]. To eliminate the nonspecific binding of monoliths to other species via electrostatic and hydrophobic interactions, the caHIgG-modified monoliths were equilibrated with a 1% BSA/PBS buffer solution. BSA, an inert protein, caps the unreacted thiol groups that are more susceptible to react with other species. BSA adsorbs at the nonspecific binding sites of the monolith surfaces with thiol terminal groups, thus increasing the chance that the only interactions that occur would be the immobilized antibody–antigen interactions.

3.3. Formation of antibody conjugated AuNPs probes

Because the sizes and shapes of AuNPs would affect their optical-physical and chemical properties, the uniform
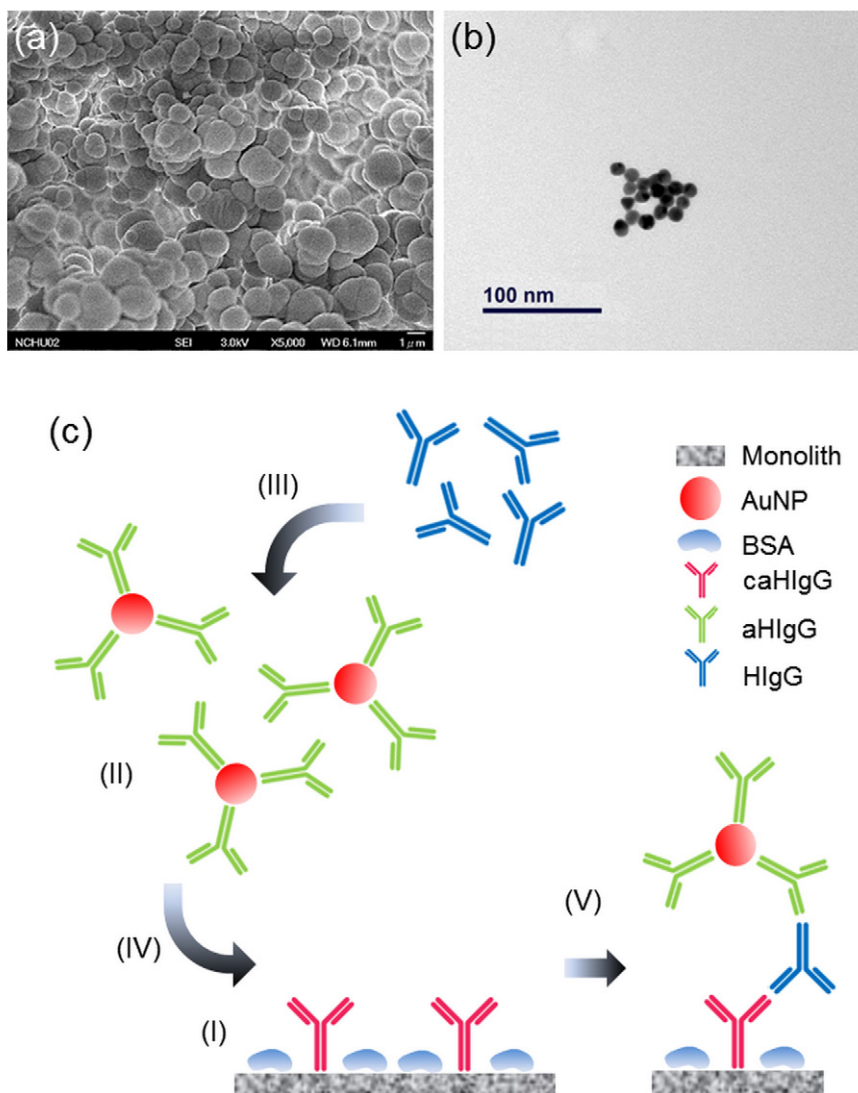
Figure 1. The sandwich immunosensing strategy using porous monolith and AuNPs probes. (a) The monoliths are photopolymerized within silica capillary forming globule clusters with a ∼1 μm diameter. (b) The AuNPs that are used in the tests are ∼13 nm in diameter, as verified via TEM images. (c) (I) The monoliths are first modified with monoclonal caHIgG and the nonspecific binding sites are eliminated by surface-attached BSA. (II) AuNP colloids are conjugated with aHIgG, followed by (III) incubating with different concentrations of HIgG. (IV) The HIgG–aHIgG–AuNPs complex is then injected into a silica capillary and (V) bound to caHIgG on the monolith surfaces. The amount of HIgG can be determined via the color variance of the bound AuNPs (red) label on the monolith (white) using a smart phone or a desktop scanner.
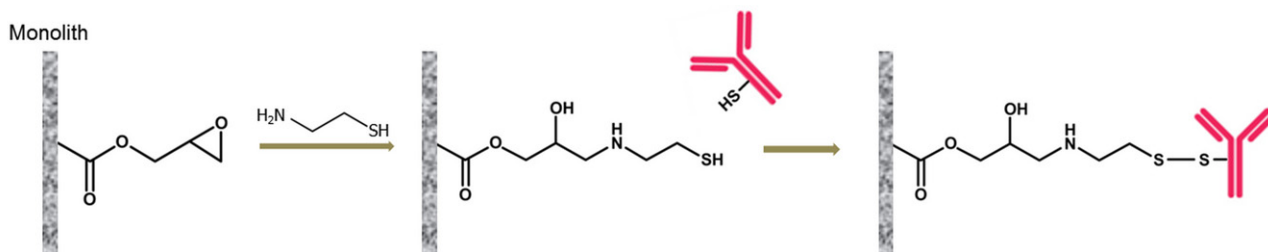
Figure 2. Immobilization of antibody on the thiolated monolith surface. Cysteamine is introduced to the poly(GMA-co-EDMA) monoliths containing oxirane moieties to open the oxirane ring and transform it into a thiol group. When the caHIgG is added, the cysteine sulfhydryl group of the caHIgG antibody can react with the thiol group on the monolith surface to form the intermolecular disulfide bridges between the antibody and the monolith.

morphology of AuNPs was characterized using TEM images. The TEM image reveals uniform sized AuNPs with a diameter of ∼13 nm (figure 1(b)).

A 10:1 molar ratio of aHIgG to AuNPs was selected based on the previous experimental results published by Ambrosi *et al* [37]. Here, we used 1 nM AuNP colloid to
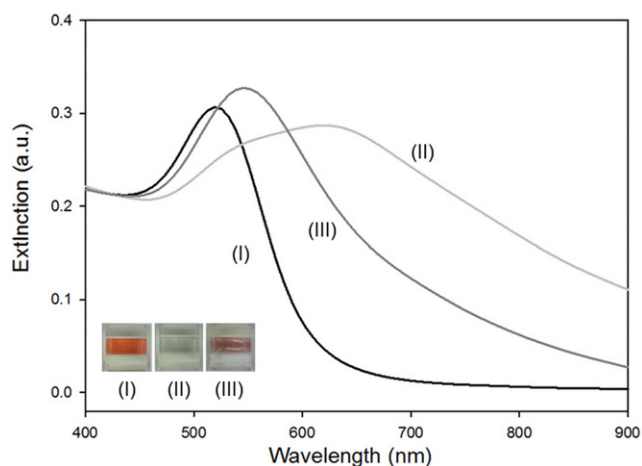
Figure 3. The visualization of AuNPs conjugated with antibodies via UV–Vis spectra. (I) The UV–Vis spectra of AuNPs have an absorbance peak at 520 nm. (II) After adding 50 mM NaCl solution to the 1 nM AuNPs colloid, the AuNPs aggregated and the absorbance peak was red-shifted to ∼625 nm. (III) However, when we modified the aHIgG antibodies on the AuNPs surface with a ratio of 10:1, the aHIgG created a steric distance, and it possessed the same surface charges as the adjacent AuNPs to avoid substantial aggregation.

mix with 10 nM aHIgG antibodies to form the aHIgG–AuNPs probes. The conjugation was further confirmed by an AuNP aggregation test (figure 3). When sufficient amounts of antibodies electrostatically attach on the AuNP surfaces, they create a steric distance and possess the same surface charges to avoid considerable aggregation when the electrolyte solution is added.

3.4. Colorimetric immunoassay characterization

The performance of the proposed immunoassay was evaluated by the colorimetric studies of the monolith. The color of the monolith was white before and after caHIgG modification (figure 4). The color of the 13 nm diameter monodispersed AuNP colloid absorbs at 520 nm as a result of the SPR effect and is red in appearance.

Upon chemical modification of the AuNPs with aHIgG, the aHIgG–AuNP complex's optical properties were slightly perturbed with the peak absorption wavelength of aHIgG–AuNPs at ∼550 nm (figure 3). Different concentrations of HIgG from 0.1 ng ml^{-1} to 1 mg ml^{-1} in 10 mM PBS buffer (pH 7.4) were added to the aHIgG–AuNPs solution to form the HIgG–aHIgG–AuNP complex. The HIgG–aHIgG–AuNPs complex was then injected into a silica capillary and incubated for 10 min. The HIgG within the HIgG–aHIgG–AuNPs complex then binds to the caHIgG that is conjugated on the monolith surfaces via antigen–antibody binding beginning from the edge of the monolith that is closest to the solution inlet. Because the capacity of the caHIgG monolith is limited and the nonspecific binding sites on the monolith surfaces have been capped by BSA, different length segments of monolith changed in color from white to dark red based on the amount of HIgG–aHIgG–AuNP that was bound to the caHIgG monolith. After rinsing with PBS
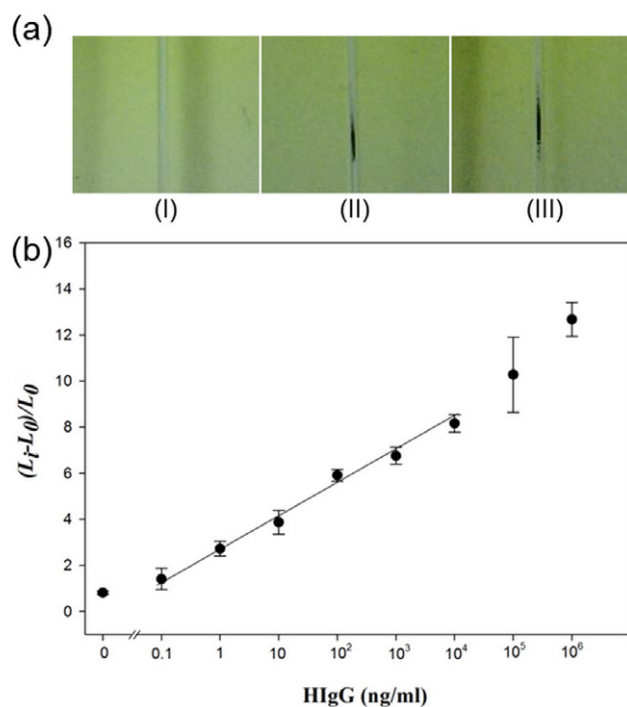
Figure 4. Porous monolith-based colorimetric immunoassay combining AuNPs probes for the detection of HIgG. (a) (I) The caHIgG-conjugated poly(GMA-co-EDMA) monolith is white. (II), (III) When 0.1 and 1 nM HIgG–aHIgG–AuNPs mixtures are injected and captured by the caHIgG-monolith surfaces, the length of the monolith segments is increased and their color changes from white to dark red. The higher concentration of HIgG leads to longer segments of monoliths that turn red. (b) A detection limit of ∼0.1 ng ml^{-1} is obtained using this immunoassay platform. The error bars represent the standard deviation from the measurements ($n = 5$). A linear correlation existed over the range of 0.1 ng ml^{-1}–10 μg ml^{-1} ($R^2 = 0.98$).

buffer to elute the residual aHIgG–AuNP, the lengths of the monolith segments with changed colors were recorded by a desktop scanner.

Figure 4 shows a plot of the length of the monolith with changed color based on the immunoassay versus the different concentrations of HIgG. The variance index of the assay is defined as

$$I = (L_i - L_0)/L_0,$$

where the L_i and L_0 are the mean colored length of the different concentrations of the injected HIgG–aHIgG–AuNPs complex and blank tests, respectively. This colorimetric immunoassay platform has a detection limit of 0.1 ng ml^{-1} with a turnaround time of 1 h. The limit of detection is defined as the concentration of a HIgG–aHIgG–AuNPs complex that produces a signal that is three times higher than the baseline noise of the control. A broad range of linear correlation exists over five orders of magnitude, from 0.1 ng ml^{-1} to 10 μg ml^{-1} ($R^2 = 0.98$). The high sensitivity and large linear dynamic range mean the assay has potential for diagnostic applications that are affordable, sensitive, specific, user-friendly, rapid and robust, equipment-free and deliverable to end-users (assured).

4. Conclusions

A new type of colorimetric immunoassay platform with improved temporal acquisition times and sensitivity has been demonstrated. We have proven that the color contrast that is created by this method can be utilized as a sensing indicator for immunoassays. Upon the formation of a monolith–AuNP complex that occurs through antigen–antibody interactions, the monoliths turned dark red. Furthermore, enzymes and substrates that are used for signaling via enzymatic reaction are not required. The detection limit of HIgG for this platform is $0.1\,\mathrm{ng\,ml^{-1}}$ with a linear correlation over a range of $0.1\,\mathrm{ng\,ml^{-1}}$–$10\,\mu\mathrm{g\,ml^{-1}}$. Additionally, the monoliths provide a shorter diffusion length between the antibodies and the mobile analytes, which improves binding efficiency and results in decreases in the incubation times that are required for antibody–antigen binding. The turnaround time of the present platform is $1\,\mathrm{h}$, which is considerably more efficient than typical sandwich assays that require $6\,\mathrm{h}$. Because the signal output is colorimetric, the assay can be performed with a desktop scanner, a smart phone or by visual inspection, thus eliminating the need for sophisticated optical equipment that is used in most conventional methods. Other colorimetric mechanisms using AuNPs for detection, such as disease diagnosis, therapy and environmental monitoring, can also be used with this platform. The colorimetric assay mechanism can also be integrated with a microfluidic platform to provide efficient and multiplexed flow control coupled with a high sensitivity, high throughput and low sample consumption point-of-care diagnostic system.

Acknowledgments

References

[1] Jaworski T *et al* 2011 *Nature* **480** E4
[2] Kepp O, Galluzzi L, Lipinski M, Yuan J Y and Kroemer G 2011 *Nature Rev. Drug Discov.* **10** 221
[3] Pai M, Zwerling A and Menzies D 2008 *Ann. Intern. Med.* **149** 177
[4] Edwards R 1999 *Immunodiagnostics: A Practical Approach* (New York: Oxford University Press)
[5] Ren L *et al* 2012 *Biosens. Bioelectron.* **35** 147
[6] Lee B S, Lee Y U, Kim H S, Kim T H, Park J, Lee J G, Kim J, Kim H, Lee W G and Cho Y K 2011 *Lab. Chip* **11** 70
[7] Ng A H C, Choi K, Luoma R P, Robinson J M and Wheeler A R 2012 *Anal. Chem.* **84** 8805
[8] Ikami M, Kawakami A, Kakuta M, Okamoto Y, Kaji N, Tokeshi M and Baba Y 2010 *Lab. Chip* **10** 3335
[9] Burger R, Reith P, Kijanka G, Akujobi V, Abgrall P and Ducree J 2012 *Lab. Chip* **12** 1289
[10] Herr A E, Hatch A V, Throckmorton D J, Tran H M, Brennan J S, Giannobile W V and Singh A K 2007 *Proc. Natl Acad. Sci. USA* **104** 5268
[11] Appleyard D C, Chapin S C and Doyle P S 2011 *Anal. Chem.* **83** 193
[12] Liu J K, Chen C F, Chang C W and DeVoe D L 2010 *Biosens. Bioelectron.* **26** 182
[13] Qin-Shu Kang X-F S, Hu N-N, Hu M-J, Liao H, Wang H-Z, He Z-K and Huang W-H 2013 *Analyst* **13** 2613
[14] Yu X *et al* 2006 *J. Am. Chem. Soc.* **128** 11199
[15] Kim S N, Rusling J F and Papadimitrakopoulos F 2007 *Adv. Mater.* **19** 3214
[16] Feng L Y, Wu L and Qu X G 2013 *Adv. Mater.* **25** 168
[17] Huang X, Yin Z Y, Wu S X, Qi X Y, He Q Y, Zhang Q C, Yan Q Y, Boey F and Zhang H 2011 *Small* **7** 1876
[18] Zheng G F, Patolsky F, Cui Y, Wang W U and Lieber C M 2005 *Nature Biotechnol.* **23** 1294
[19] Tok J B H, Chuang F Y S, Kao M C, Rose K A, Pannu S S, Sha M Y, Chakarova G, Penn S G and Dougherty G M 2006 *Angew. Chem. Int. Edn Engl.* **45** 6900
[20] Mayilo S, Kloster M A, Wunderlich M, Lutich A, Klar T A, Nichtl A, Kurzinger K, Stefani F D and Feldmann J 2009 *Nano Lett.* **9** 4558
[21] Mani V, Chikkaveeraiah B V, Patel V, Gutkind J S and Rusling J F 2009 *ACS Nano* **3** 585
[22] Azzazy H M E and Mansour M M H 2009 *Clin. Chim. Acta* **403** 1
[23] Rosi N L and Mirkin C A 2005 *Chem. Rev.* **105** 1547
[24] Daniel M C and Astruc D 2004 *Chem. Rev.* **104** 293
[25] Myroshnychenko V, Rodriguez-Fernandez J, Pastoriza-Santos I, Funston A M, Novo C, Mulvaney P, Liz-Marzan L M and de Abajo F J G 2008 *Chem. Soc. Rev.* **37** 1792
[26] Takeuchi Y, Ida T and Kimura K 1996 *Surf. Rev. Lett.* **3** 1205
[27] Zhao W, Brook M A and Li Y F 2008 *ChemBioChem* **9** 2363
[28] Fan C H, Wang S, Hong J W, Bazan G C, Plaxco K W and Heeger A J 2003 *Proc. Natl Acad. Sci. USA* **100** 6297
[29] Dulkeith E, Morteani A C, Niedereichholz T, Klar T A, Feldmann J, Levi S A, van Veggel F C J M, Reinhoudt D N, Moller M and Gittins D I 2002 *Phys. Rev. Lett.* **89** 203002
[30] Svec F and Frechet J M J 1996 *Science* **273** 205
[31] Peters E C, Petro M, Svec F and Frechet J M J 1998 *Anal. Chem.* **70** 2288
[32] Liu J K, Chen C F, Tsao C W, Chang C C, Chu C C and Devoe D L 2009 *Anal. Chem.* **81** 2545
[33] Horejsi R, Kollenz G, Dachs F, Tillian H M, Schauenstein K, Schauenstein E and Steinschifter W 1997 *J. Biochem. Biophys. Methods* **34** 227
[34] Parolo C, de la Escosura-Muniz A and Merkoci A 2013 *Biosens. Bioelectron.* **40** 412
[35] Rogers A B, Cormier K S and Fox J G 2006 *Lab Invest.* **86** 526
[36] Xu Y, Cao Q, Svec F and Frechet J M J 2010 *Anal. Chem.* **82** 3352
[37] Ambrosi A, Castaneda M T, Killard A J, Smyth M R, Alegret S and Merkoci A 2007 *Anal. Chem.* **79** 5232
[38] Grabar K C, Freeman R G, Hommer M B and Natan M J 1995 *Anal. Chem.* **67** 735
[39] Jin R C, Wu G S, Li Z, Mirkin C A and Schatz G C 2003 *J. Am. Chem. Soc.* **125** 1643
[40] Preinerstorfer B, Bicker W, Lindner W and Lammerhofer M 2004 *J. Chromatogr.* A **1044** 187